[*Hung * et al., 5(2): February, 2018*]

ISSN: 2349-5197
Impact Factor: 3.765

INTERNATIONAL JOURNAL OF RESEARCH SCIENCE & MANAGEMENT

EFFECTS OF ROTARY SWAGING ON MICROSTRUCTURE AND MECHANICAL PROPERTIES OF 2024 ALUMINUM TUBES

Chia-Wei Lin, Fei-Yi Hung* & Truan-Sheng Lui, Hsuan-Po Chen
Department of Materials Science and Engineering, National Cheng Kung University, Tainan 701, Taiwan

DOI: 10.5281/zenodo.1168822

Keywords: rotary swaging; 2024 aluminum alloy; tensile mechanical properties; T6 heat treatment.

Abstract
Rotary swaging is a process usually applied to reduce the entire or local diameter and size of rods and tubes. The effects of the rotary swaging process and subsequent T6 heat treatment are investigated in this research. The results show that rotary swaging process refines grain size, decreases the eutectic phase fraction, enhances mechanical strength, and decreases mechanical elongation. After suitable T6 heat treatment, the as-swaged 2024 tube had the highest tensile strength; its yield stress reached about 350 MPa. The factors that affect mechanical properties are remaining residual stress, internal defects, precipitation, and grain size refinement. This study proves that rotary swaging process improves mechanical strength in addition to reducing dimensions.

Introduction
Rotary swaging, which is usually used for reducing the entire or local diameter of tubes and rods, is a process that utilizes short strokes at high frequency and small deformation. The advantages of this process include surface quality enhancement, material savings, and leading time shortness [1-3]. It can be used at high temperatures or room temperature and is usually applied to low-ductility materials such as high-strength steels and superalloys.
The effects of rotary swaging process have been extensively investigated. When rotary swaging was applied in steel tube forging, surface hardness increased and surface roughness improved [4]. When it was applied to 1050 aluminum alloys, tensile strength increased and tensile ductility dropped severely due to high dislocation accumulation [5]. When it was applied to Mg alloys, the basal plane of the Mg lattice became parallel to the direction of swaging, showing that rotary swaging affects texture [6]. When rotary swaging process was applied to 5083 aluminum alloys, the grains of the eutectic phases were refined [7]. In the present study, rotary swaging process is applied to 2024 aluminum extruded tubes.
2024 aluminum alloy is an Al-Cu alloy that is precipitation-hardened. The major precipitated phase is Al_2Cu (θ phase). It is often used in the aerospace industry and some structural components because of its high strength and high fatigue resistance.
The major alloying elements of 2024 aluminum alloy are Cu and Mg. The kinds of major precipitation hardening phase are determined based on the Cu/Mg ratio. The major precipitation hardening phase is only Al_2CuMg (s phase) when the Cu/Mg ratio is below 2.6; Al_2Cu (θ phase) and Al_2CuMg (s phase) co-exist as major precipitation phases when the Cu/Mg ratio is above 2.6 [8]. The ternary eutectic temperature of Al, Mg, and Cu is 507 °C. The limits of the solid solubility of Mg and Cu in the Al matrix are 1.6 wt.% and 4.1 wt.%, respectively. Besides Cu and Mg, Mn, Si, and Fe are added to this alloy. Adding Mn can inhibit grain growth, enhance strength, and increase recrystallization temperature. However, the grain boundaries become weak and brittle when the content of Mn is above 1 wt.% [9-10]. Adding Fe is beneficial for extrusion and the formation of Al_7Cu_2Fe (N phase). Adding Si can increase the number of nucleation sites of precipitated phases and improve castability [8].
T6 heat treatment is the most general heat treatment for enhancing heat-treatable aluminum alloys such as 2xxx, 6xxx, and 7xxx series alloys. It includes two steps: solution treatment and artificial aging treatment. During artificial aging, the major precipitation phase changes and transforms with the composition and aging duration. For the 2xxx series, with increasing Mg content, the major precipitation phase transforms from Al_2Cu (θ phase) to Al_2CuMg (s phase). The precipitation sequence with increasing aging time is as follows:

I. S.S.S.S. → G.P. zones→ θ'' → θ'→ θ
II. S.S.S.S. → G.P.B. zones→ S'' → S'→ S

where S.S.S.S. is supersaturated solid solution, G.P. zones are aggregated clusters of Cu atoms, the coherent θ'' phase and the semi-coherent θ' phase are metastable Al_2Cu, and the incoherent θ phase is stable Al_2Cu. G.P.B. zones are aggregated clusters of Cu and Mg atoms, the coherent S'' phase and the semi-coherent S' phases are metastable Al_2CuMg, and the incoherent S phase is the stable Al_2CuMg phase [11]. The strengthening mechanism relies mainly on the strain field generated by the precipitation phases restricting dislocation slipping. The degree of restriction by the coherent and semi-coherent phases is higher than that by the coherent phases. Therefore, in 2xxx series aluminum alloys, since the major precipitation phase is a coherent or semi-coherent phase such as θ'', θ', S'', or S', the strengthening effect is obvious. In theory, the highest strengthening effect can be achieved by using suitable solution treatment and peak artificial aging to obtain large amounts of precipitation hardening phases (e.g., G.P. zones, θ', or S') in the matrix.

In this research, the microstructural characteristics, mechanical properties (estimated from a tensile test), and fracture mechanism of rotary-swaged 2024 aluminum extruded tubes treated with T6 heat treatment were investigated and compared with those of as-received 2024 aluminum tubes to understand the effect of rotary swaging on the microstructure evolution and mechanical performance of such tubes. The strengthening mechanism of rotary swaging process is discussed and the potential of using this process to strengthen aluminum alloys is demonstrated.

Materials and experimental methods

The rotary swaging process is a common technique used for reducing the diameter of rods or tubes. An illustration of the process is shown in Fig. 1, where A is a supporting ring, B is a pressure roller, C is a thrust piece, and D is a swaging die. In this research, the workpiece is a tube. Extruded tubes are plunged into the center of the swaging machine with a mandrel with suitable diameter. As the swaging machine works, swaging dies (D) and thrust pieces (C) rotate around the swaging axle at high frequency. When pressure rollers push the thrust pieces, the swaging dies (D) hit and deform the tube. The rotation continues at a high rotation rate, resulting in a large number of small deformations on the tube with each short stroke. The rotation rate, which also represents the swaging rate, can reach about 6000 rpm. In this study, the rotation rate of the swaging machine is 2500 rpm. The workpieces are also rotated and plunged at a stable feeding speed in the rotary swaging process to enhance the uniformity of deformation. In this study, the rotation rate of the tube is 100 rpm and the feed speed is set to 50 mm/min.

Table 1 Chemical composition of 2024 aluminum tubes

Element	Cu	Mg	Mn	Si	Fe	Cr	Zn	Ti	Al
wt.%	4.18	1.52	0.63	0.14	0.15	0.01	0.07	0.02	Bal.

The initial material used in this research is an extruded 2024 aluminum tube subjected to stress relief annealing. It is designated as F. Its composition, determined using a glow dispersive spectrometer, is shown in Table 1. The weight percentages of the major alloying elements are about 4.2% Cu, 1.5% Mg, 0.6% Mn, 0.1% Si, and 0.1% Fe. Stress relief annealing was used to decrease the strength of swaging workpieces to prolong the life of the swaging machine parts. The as-received 2024 aluminum tubes were heated in an air furnace at 430 °C for 2 hours and then cooled in the air furnace at a slow cooing rate to room temperature. The rotary-swaged tube is designated as RS. The dimensions of these two materials are shown in Fig. 2(a). The thickness, outer diameter, and inside diameter of F (as-annealed tubes) are 5, 35, and 30 mm, respectively. Those of RS (as-swaged tubes) are 2.7, 29.7, and 27 mm, respectively. The area-shrinking ratio of the rotary swaging process is about 60%. The definitions of "directions" are shown in Fig. 2(b). Three directions, namely extrusion direction (ED), normal direction (ND), and transverse direction (TD), are defined to indicate which plane or direction was observed along.

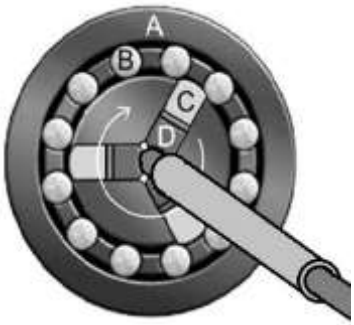

Fig. 1 Illustration of rotary swaging equipment.

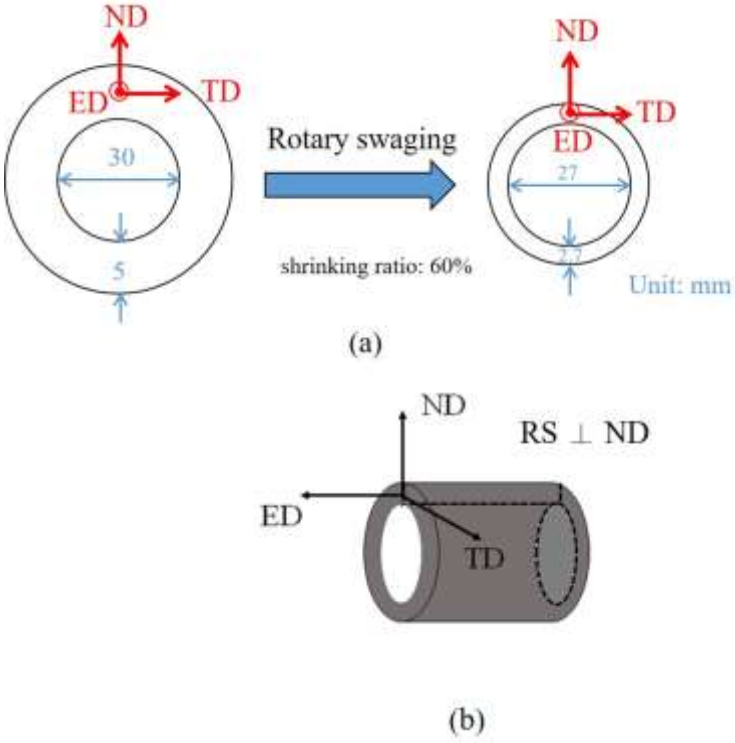

Fig. 2 (a) Dimensions of as-received 2024 tubes and as-swaged 2024 tubes and (b) definitions of directions.

2024 Al alloy is a heat-treatable alloy. T6 heat treatment, which includes solution heat treatment and artificial aging treatment, was used to improve the hardness and strength of alloys in this study. The effects of T6 heat treatment on the microstructural characteristics and mechanical properties of as-annealed materials (F) and as-swaged materials (RS) are compared. The conditions used for T6 heat treatment are discussed in Section 3.1. The optimal conditions for T6 heat treatment (solution heat treatment temperature and artificial aging temperature and time) were determined using the Rockwell hardness (HR) test. The measurement conditions for HR followed the F-scale. The loading was 60 kgf and the indenter was a 1/16-inch (0.159-cm) steel sphere.

In order to investigate the effects of rotary swaging and T6 heat treatment on the microstructural evolution of 2024 aluminum alloys, the specimens were polished and etched for metallographic observation. An optical microscope (OM) was used to observe the morphology of materials and ImageJ software (NIH, Bethesda, MD) was used to calculate and quantify the area fraction of eutectic phases to estimate the solid solution degree. Electron probe X-ray microanalysis (EPMA) was used to understand the effects of rotary swaging and T6 heat treatment on the distributions of elements and phases.

F, RS, T6-heat-treated F, and T6-heat-treated RS were analyzed using X-ray diffraction (XRD) to discuss the effects of rotary swaging process and heat treatment on 2024 aluminum alloy texture. The scan rate was set as 4°/min and the scan angle range was set from 20° to 90°. ED and ND were the analyzed directions. XRD was also used to investigate the residual stress of materials [12-13]. ED was the analyzed direction. The analyzed peak was (331), whose 2θ angle is 112.05°.

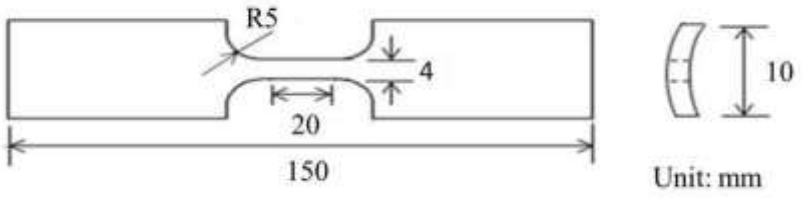

Fig. 3 Dimensions of tensile specimens.

Finally, the mechanical properties, which include micro-hardness and tensile properties, of F, RS, T6-heat-treated F, and T6-heat-treated RS were investigated. The micro-hardness was measured using the Vickers hardness (HV) test. The full load was 100g; the load was applied for 10 s. A universal material tester was used for the tensile test, which was conducted at room temperature, with the initial strain rate set at 1.67×10^{-3} s^{-1}. The dimensions of the tensile specimens are shown in Fig. 3. The gauge length is 20 mm. The thicknesses of the specimens are 5 mm (before rotary swaging process) and 2.7 mm (after rotary swaging process). The tensile direction is parallel to the ED direction. Each datum is the average of at least three samples. After the tensile test, the mechanism of tensile fracture was analyzed. The analysis included two parts: (i) the fracture surface of fracture specimens was observed using scanning electron microscopy (SEM) and energy-dispersive X-ray spectrometry (EDS); (ii) the subsurface morphologies of fracture specimens were observed using OM after mounting and polishing.

Results and discussion

Conditions for T6 heat treatment

The T6 heat treatment process commonly consists of three steps: (1) solution heat treatment, (2) water quenching, and (3) artificial age hardening. In the solutionizing step, the alloy should be heated to a temperature just below the incipient melting point for an adequate duration to allow all the solute atoms to dissolve to form a single-phase solid solution. Subsequently, quenching in water (below 60 °C) at an adequate cooling rate is used to inhibit the formation of Mg-Si precipitates, resulting in a supersaturated solid solution.

The incipient melting temperature of rotary-swaged 2024 aluminum tubes (RS) was investigated using differential scanning calorimetry (DSC). The results are shown in Fig. 4. The first endothermic peak appears at 495 °C. This indicates that partial melting starts at about 495 °C. Therefore, the solution heat treatment temperature was set to 490 °C for 2 hours at first. Artificial aging curves were obtained at temperatures of 170 °C, 190 °C, 210 °C, and 230 °C. The curves show the hardness evolution with increasing aging time (see Fig. 5(a)). The peak aging duration decreases with increasing aging temperature. When the artificial aging temperature is 210 °C, the peak aging hardness is highest. This is thus the optimal artificial aging temperature for enhancing hardness. The peak aging located at a holding duration of 3 hours at 210 °C artificial aging.

ISSN: 2349-5197
Impact Factor: 3.765

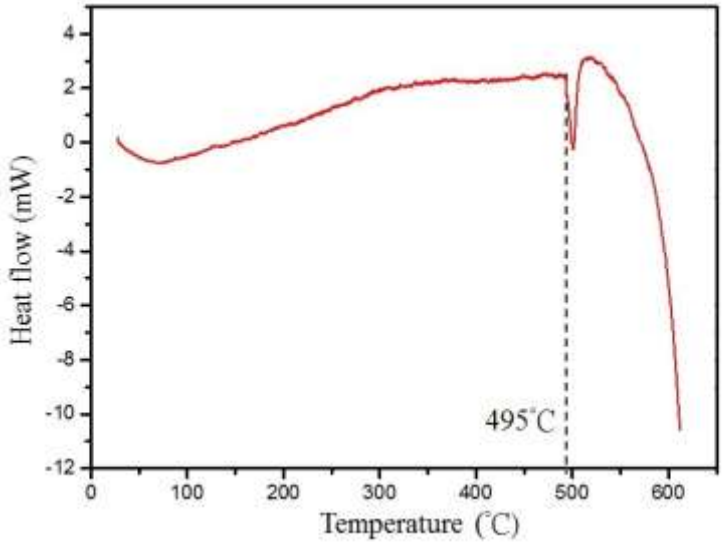

Fig. 4 DSC curve of as-received 2024 Al alloy (F).

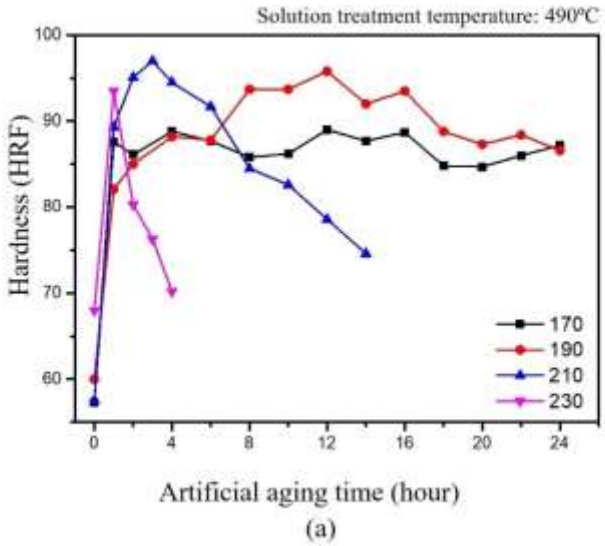

(a)

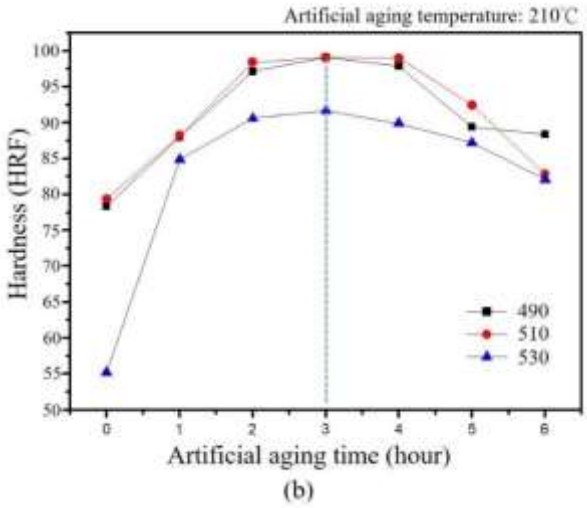

Fig. 5 Artificial aging curves for various (a) artificial aging temperatures and (b) solution temperatures.

The temperature of solution heat treatment is discussed here since the amount of solid solution can be affected by solid solution temperature. In theory, the amounts of precipitation phases increase with increasing amount of solid solution. The relief-annealed 2024 aluminum (F) is used here to discuss the effects of solid solution temperature. The solid solution temperature was set at 490 °C, 510 °C, and 530 °C, with a holding duration of 2 hours. The artificial aging temperature was set at 210 °C based on Fig. 5(a). Figure 5(b) shows artificial aging curves for three solid solution temperatures. The results reveal that hardness is lowest when the solid solution temperature is 530 °C for a given artificial aging duration. This is likely due to many second phases with low melting points melting to become liquid phases at 530 °C for 2 hours and a lot of voids forming during water quenching due to severe volume shrinking during solidification. These voids greatly reduce hardness. Figure 5(b) also reveals that the peak aging both located at a holding duration of 3 hours at 490 °C and 510 °C solid solutionizing. The hardness values at peak aging for the two solid solution temperatures are almost identical. The results show the suitable for this two alloys, the relief-annealed 2024 aluminum tube (F) and the rotary-swaged 2024 aluminum tube (RS), are the same..

Based on the above experimental results, 490 °C for 2 hours and 510 °C for 2 hours were chosen as the conditions for solid solution treatment and 210 °C for 3 hours was chosen as the conditions for artificial aging. The T6-heat-treated F and RS tubes are designated as F490AA, F510AA, RS490AA, and RS510AA, respectively.

Microstructural characteristics and phase identification

The microstructures of six specimens (F, RS, F490AA, F510AA, RS490AA, and RS510AA) are shown in Figs. 6 and 7. Figure 6 shows the etched metallographic images in the ED direction of F and RS. Both fine and coarse grains exist in F, as shown in Fig. 6(a), but only fine grains exist in RS, as shown in Fig. 6(b). These results show that rotary swaging process can uniformly refine all alloy grains, which is likely due to dynamic recrystallization in the rotary swaging process. According to the grain coalescence mechanism, if the crystal orientations of neighboring grains are similar, the grains will easily merge, forming coarse grains. This led to the non-uniform grain distribution in F.

Figure 7 shows the etched microstructures of F490AA, F510AA, RS490AA, and RS510AA. According to the three-dimensional metallographic images of these four samples (Figs. 7(a-d), respectively), the grains grew after T6 heat treatment, with the grain sizes of RS490AA and RS510AA being smaller than those of F490AA and F510AA. The grain growth likely occurred in the solution treatment step due to its high temperature. The figures also show that the microstructures of these four specimens are anisotropic. The major axis of the grains is parallel to the extrusion direction. The major axis of heat-treated extrusion specimens (F490AA and F510AA) is longer than that of heat-treated rotary-swaged specimens (RS490AA and RS510AA). In other words, the rotary swaging

process decreases the level of anisotropy but cannot diminish the texture of extruded samples. Figures 7(e) and (f) show magnified metallographic images in the ED direction of F490AA and F510AA, respectively. The results demonstrate that the grains are still non-uniform after T6 heat treatment; both coarse and fine grains exist in the heat-treated extrusion alloys.

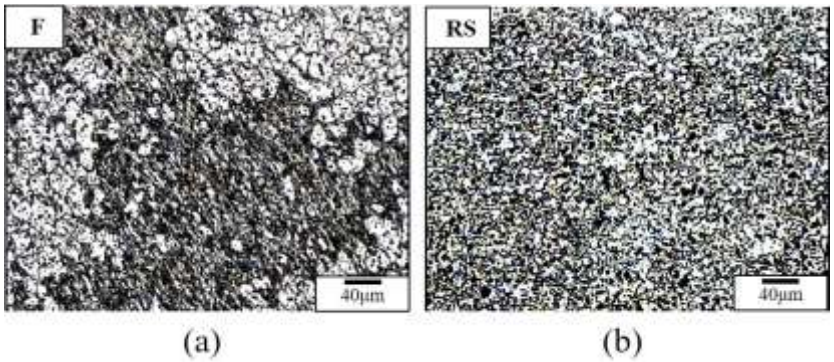

Fig. 6 Microstructures of (a) F and (b) RS (ED direction).

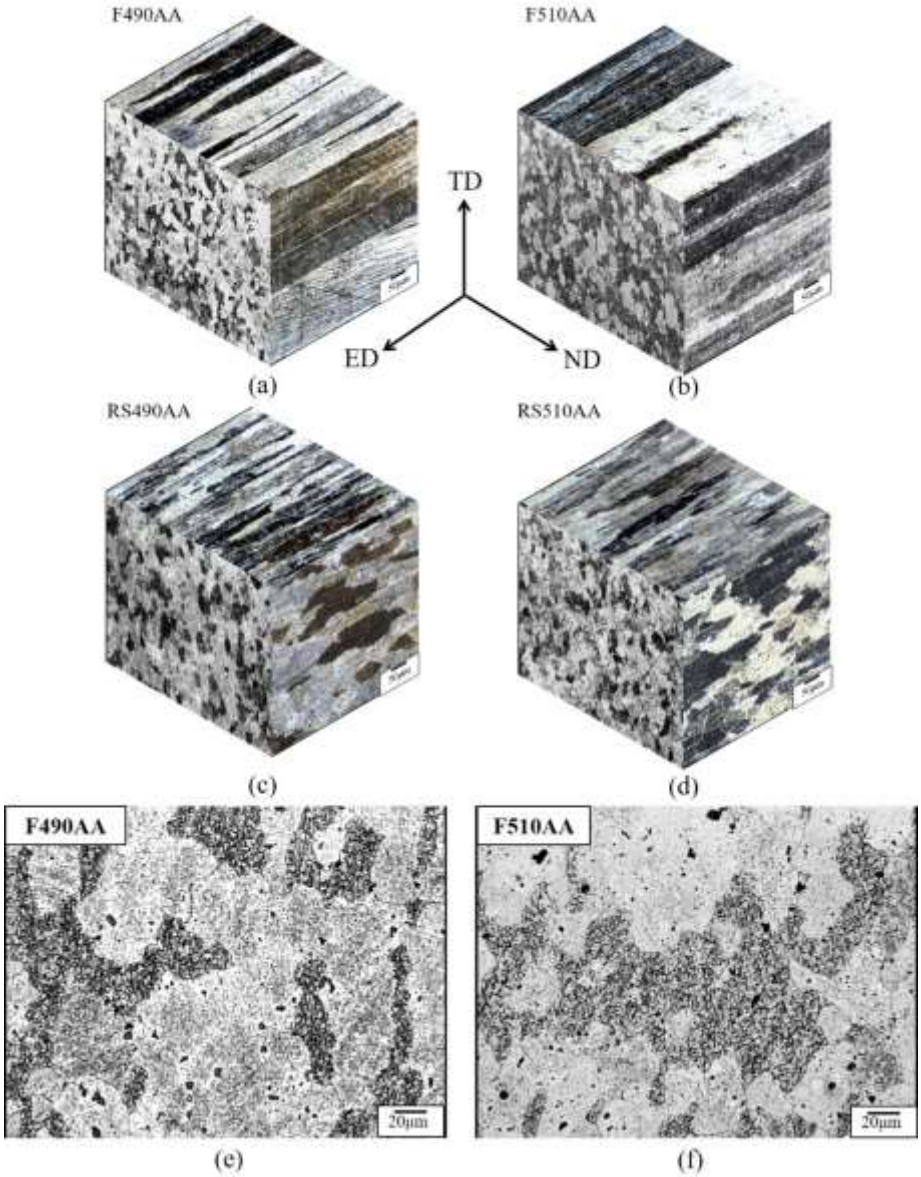

Fig. 7 Three-dimensional metallographic images of (a) F490AA, (b) F510AA, (c) RS490AA, and (d) RS510AA and ED-directional microstrucures of (e) F490AA and (f) F510AA.

OM metallographic images without etching were obtained of the six specimens for calculating the area fraction of eutectic phases to understand the solid solution effects of solution temperature and rotary swaging process on the eutectic phases in as-received aluminum tubes. Because precipitated phases are too small to observe in OM images, the fraction of eutectic phases were calculated and the degree of solid solution was quantified. A lower fraction of eutectic phases indicates a higher degree of solid solution. In general, a higher degree of solid solution leads to stronger precipitation hardening. The images are shown in Fig. 8 and the eutectic phase fractions are shown in Fig. 9. These results reveal that the fraction of eutectic phases drops severely after T6 heat treatment. The eutectic phases were mainly dissolved in the solid solution heat treatment step because of its high temperature. A higher solid solution temperature allows more of the eutectic phases to dissolve. In addition, the eutectic phase fraction of RS (8.6%) is 2.3% lower than that of F (10.9%). It should due to that The rotary swaging process can refine particle phases in materials. This led to higher amounts of solid solution. Thus, the eutectic phase fraction of RS490AA (1.4%) is slightly less than that of F490AA (2.3%) and that of RS510AA (1.2%) is slightly less than

that of F510AA (1.4%). These results show that rotary swaging process reduces the fraction of eutectic phases before and after T6 heat treatment. Rotary swaging process enhances the degree of solid solution.

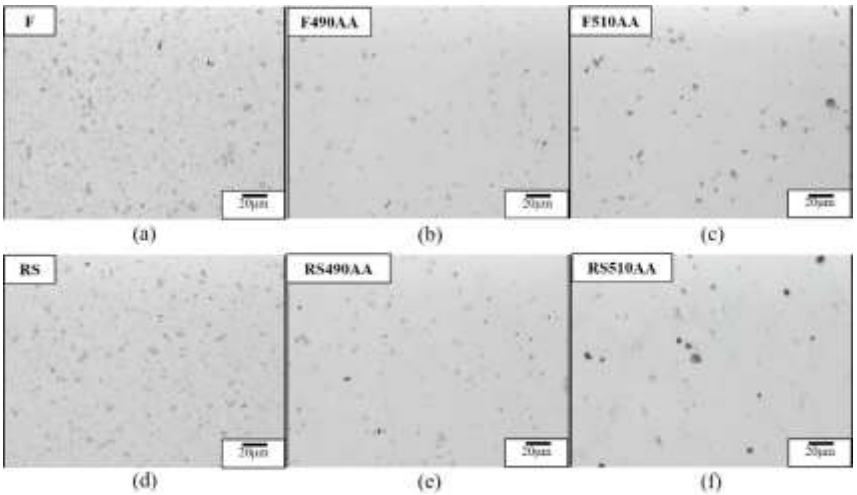

Fig. 8 Microstructures without etching for eutectic phase observation (ED plane) of (a) F, (b) F490AA, (c) F4510AA (d) RS, (e) RS490AA, and (f) RS510AA.

EPMA was used to investigate and identify the eutectic phases in six kinds of specimen. The results are shown in Fig. 10. The kinds of eutectic phase are the same in all specimens. Four kinds of eutectic phase, namely a compound of Cu and Mg, a compound of Cu, Fe, and Mn, a compound of Mg and Si, and Si particles, appear in the EPMA data. After T6 heat treatment, the eutectic phases dissolved into the Al matrix but did not transform into other phases. Based on previous research [12] and the above results, these four eutectic phases are Al_2CuMg (S phase), Al_7Cu_2Fe(Mn) (N phase), Mg_2Si (β phase), and Si particles.

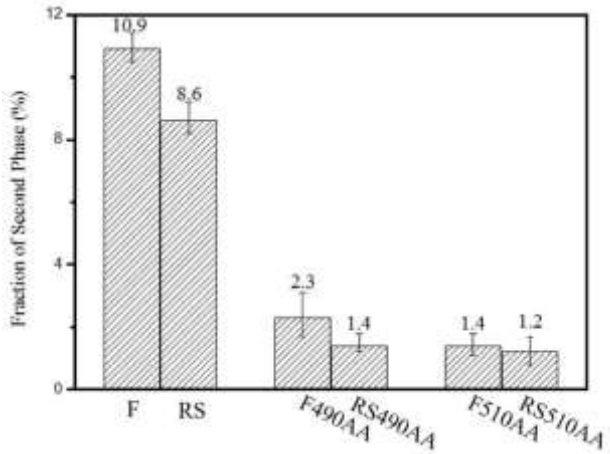

Fig. 9 Phase fractions of eutectic phases.

ISSN: 2349-5197
Impact Factor: 3.765

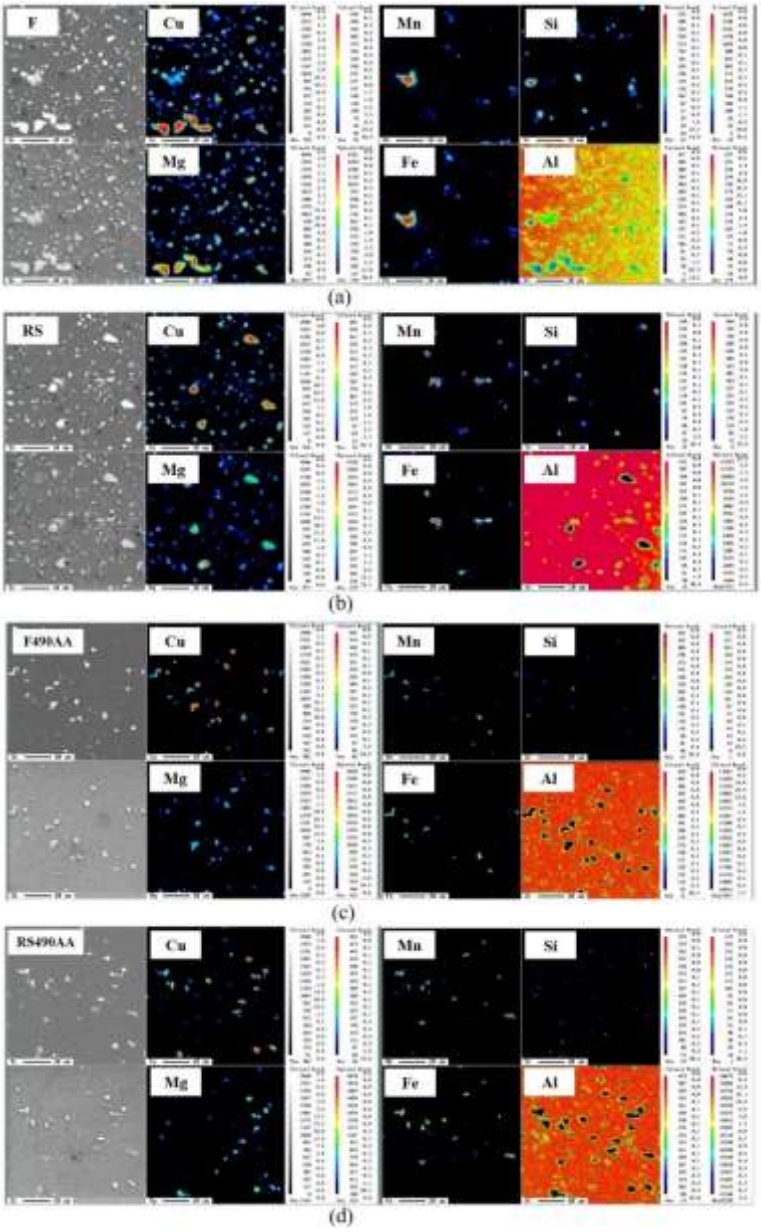

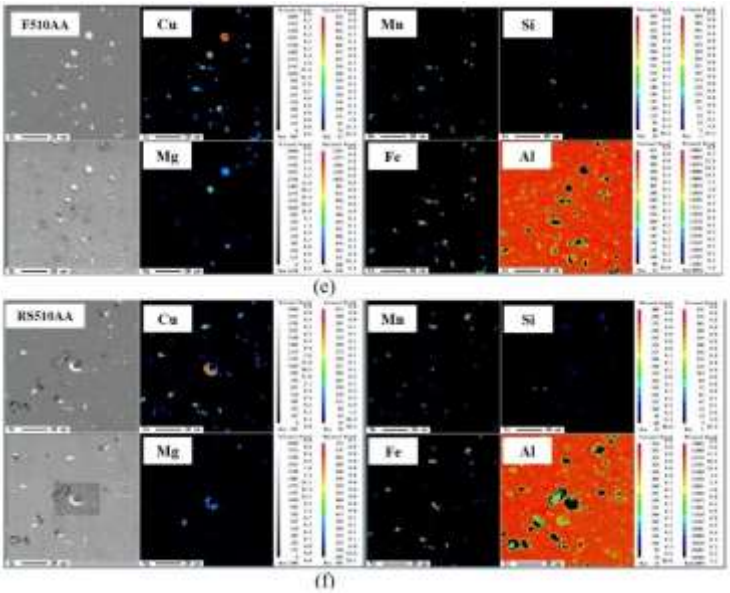

Fig. 10 Elementary distribution estimated from EPMA of (a) F, (b) F490AA, (c) F4510AA (d) RS, (e) RS490AA, and (f) RS510AA.

Figure 11(a) shows that some voids existed in RS510AA. This is due to the eutectic phases of RS510AA partially melting in the solid solution step at 510 °C. High-density dislocation aggregation leads to a decrease of the melting point of phases (eutectic phases)[13]. The occurrence of partial melting indicates that the rotary swaging process introduces large numbers of dislocations into the aluminum alloy. This is verified by the phase transformation temperature data of extruded alloys (F) and rotary-swaged alloys (RS) obtained using DSC, shown in Fig. 11(b). The figure shows that the endothermic peak of RS is slightly left-shifted to a temperature lower than that for F.

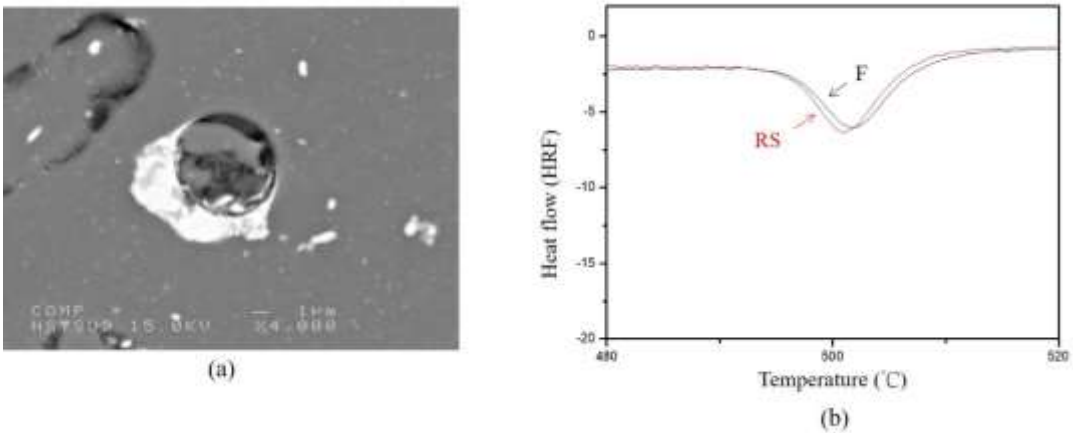

Fig. 11 (a) Morphology of partial melting phases in RS and (b) DSC curves of F and RS.

Effects of rotary swaging on mechanical performance

The micro-hardness distributions of F, RS, RS490AA, and RS510AA were estimated to determine whether the rotary swaging process resulted in a non-uniform distribution of micro-hardness, which would degrade mechanical properties. Moreover, if rotary swaging process does degrade mechanical properties, it was investigated whether T6 heat treatment can make the distribution of micro-hardness uniform. The micro-hardness data are shown in Fig. 12. The distance (x-axis value) in this figure is defined as the distancefrom the inside wall of the tube. The figure shows that the micro-hardness distribution of F is uniform. After the rotary swaging process, the micro-

hardness distribution becomes non-uniform (55-85HV). The outer part of the swaged tubes is much harder than the inner part. This occurs because with the rotary swaging process, deformation is introduced from the outside in. Notably, after T6 heat treatment, the micro-hardness distribution of swaged tubes becomes uniform. This shows that T6 heat treatment diminishes the non-uniformity of swaged tubes. The micro-hardness distribution of T6-heat-treated swaged tubes does not affect mechanical performance.

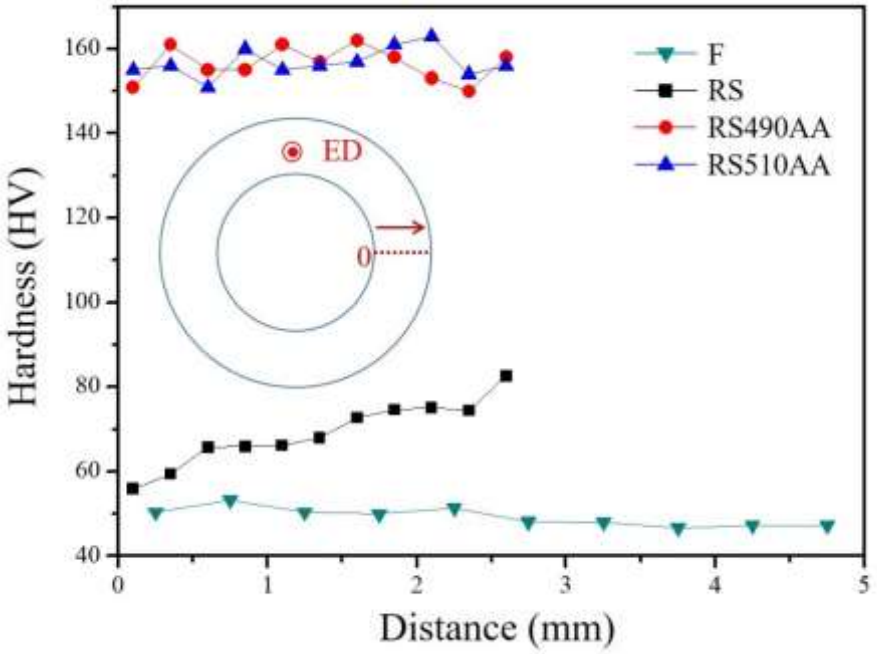

Fig. 12 Distribution of hardness of materials.

Figure 13 shows tensile flow curves and Fig. 14 shows tensile strength and tensile elongation for six specimens. The detailed values of tensile strength and tensile elongation are shown in Table 2.

Table 2 Mechanical properties of alloys

Material	YS (MPa)	UTS (MPa)	UE (%)	TE (%)
F	111.6	198.3	16.3	25.7
RS	200.2	236.6	1.5	4.2
F490AA	264.7	440.4	15.6	18.0
RS490AA	332.6	453.3	8.5	10.0
F510AA	285.7	463.7	8.5	13
RS510AA	349.4	485.2	7.3	9.0

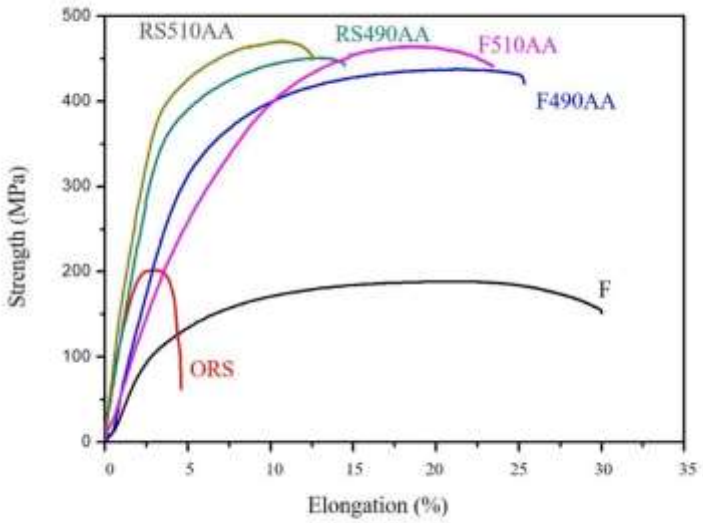

Fig. 13 Tensile flow curves of various materials.

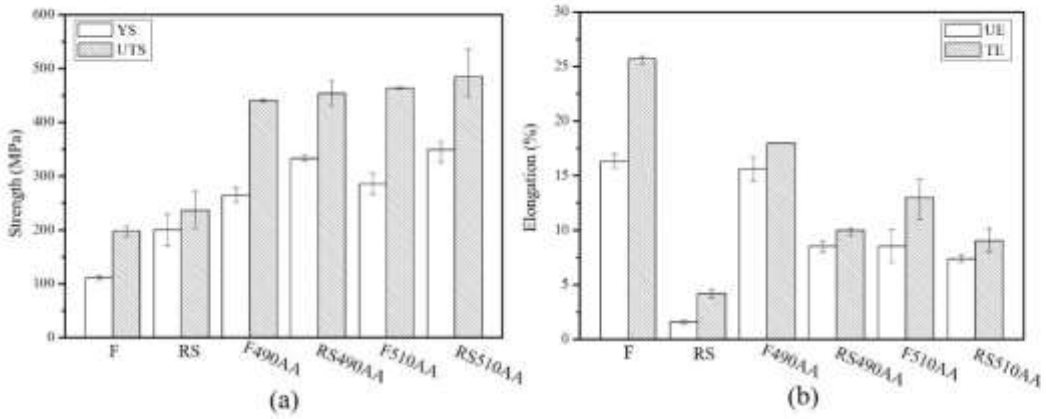

Fig. 14 Tensile mechnical properties: (a) strength and (b) elongation.

The results indicate that the rotary swaging process increases tensile strength, especially yield stress (YS), which increases from 111.6 to 200.2 MPa, but greatly decreases tensile ductility. The uniform elongation (UE) and total elongation (TE) of the as-swaged alloy (RS) are only about 20% of those of the as-received alloy (F). This is due to the rotary swaging process introducing a large number of dislocations [14-15], resulting in an increase in tensile strength and a large drop in tensile elongation. The tensile strength of heat-treated alloys (F490AA, F510AA, RS490AA, and RS510AA) is much higher than that of the original alloys (F and RS). This demonstrates that T6 heat treatment enhances the tensile strength of as-received alloys and as-swaged alloys. A higher solid solution temperature leads to higher ultimate tensile stress (UTS) and YS. The tensile elongation of alloys exhibits the opposite trend. These results are consistent with the eutectic phase fraction data shown in Figs. 8 and 9. A higher degree of solid solution, resulting from a higher solid solution temperature, leads to stronger precipitation hardening. UTS values follow the order (from high to low) $UTS_{RS510AA}$, UTS_{F510AA}, $UTS_{RS490AA}$, UTS_{F490AA},

UTS_{RS}, and UTS_F, and YS values follow the order $YS_{RS510AA}$, $YS_{RS490AA}$, YS_{F510AA}, YS_{F490AA}, YS_{RS}, and YS_F. The data show that even though a few partial melting voids appeared in RS510AA, as shown in Fig. 11, these voids did not affect the order of tensile strength. RS510AA had the highest tensile strength, with a UTS of 485.2 MPa and a YS of 349.4 MPa. The YS and UTS values of as-swaged alloys are higher than those of as-received aluminum tubes after T6 heat treatment for a given solution temperature; those of RS490AA are larger than those of F490AA and those of RS510AA are large than those of F490AA. This demonstrates that the tensile strength can be improved by rotary swaging process. Notably, the YS values of RS510AA (349.4 MPa) and RS490AA (332.6 MPa) are much higher than those of F510AA (285.7 MPa) and F490AA (264.7 MPa). Higher yield strength means higher resistance to deformation. In many applications, such as structural components for architecture and cars, any deformation is unacceptable. The data show that the rotary swaging process enhances deformation resistance. It thus not only reduces the diameter of tubes and rods, but also improves yield stress. However, rotary swaging process decreases tensile ductility. The tensile ductility (uniform elongation and total elongation) of as-swaged tubes is lower than that of as-received tubes before and after T6 heat treatment at two solution temperatures. The trend of ductility is opposite to that of strength. However, the ductility of RS490AA and RS510AA does not affect their applicability as structural materials because high ductility is important for forming.

According to previous researches [16-17] and our experimental analysis, the following factors may have promoted the mechanical properties, especially YS, in the rotary swaging process. (1) The effect of residual stress: in the XRD analysis, a positive value means tensile residual stress and a negative value means compressive residual stress. Figure 15(a) shows the residual stress direction. The direction of the frequent strokes of rotary swaging is parallel to the ND direction (swage on the outside tube wall), resulting in compressive residual stress in the ND direction. Therefore, the residual stress in the ED direction analyzed using XRD should be tensile stress. The residual stress values in the ED direction for F, RS, F510AA, and RS510AA are shown in Fig. 15(b) and Table 3. The initial residual stress of the as-received tubes is -20.8 MPa. After T6 heat treatment, the compressive residual stress decreases to -4 MPa due to the solid solution treatment at 510 °C, which is high enough to release almost all the internal stress. After rotary swaging process, the residual stress became +35.2 MPa. This reveals that rotary swaging introduced high tensile residual stress into specimens in the ED direction due to the formation of high-density dislocations, which increase strength but greatly decrease elongation. After the as-swaged specimen was subjected to T6 heat treatment, the residual stress became +16.2 MPa. This indicates that some dislocations vanished after heat treatment. The remaining dislocations restricted dislocation slip, increasing the yield strength before tensile deformation. RS510AA thus had a higher yield strength and lower elongation than those of F510AA. (2) The effect of internal defects: according to the literature [16-17], the full width at half maximum (FWHM) of XRD patterns can be used to investigate the internal defects in materials. Materials with more internal defects (e.g., voids, dislocations, and stacking faults) exhibit a broader FWHM and possibly higher strength. The XRD analysis results for the ED direction of six specimens are shown in Fig. 16(a); these results were normalized using the (111) peak. Figure 16(b) shows a magnified view around the (111) peak of Fig. 16(a). The FWHM values at the (111) peak for RS490AA and RS510AA are broader than those for F490AA and F510AA; the rotary swaging process thus introduced defects, as indicated by a broader FWHM, even after heat treatment. In theory, these defects should be nucleation sites for precipitation in the artificial aging step because inhomogeneous nucleation free energy is lower than that of homogeneous nucleation. The defects increase the number of nucleation sites and lead to the uniform nucleation and refinement of precipitation phases, resulting in a higher degree of precipitation hardening. This improves mechanical strength, especially YS. In addition, these defects also explain why the residual stress values of RS, RS490AA, and RS510AA are larger than those of other specimens. (3) The effect of precipitation phase content: Fig. 16(b) shows that the scattering angles at (111) for F490AA and F510AA are smaller than those for RS490AA and RS510AA. This result can be explained using Bragg's law, whose formula is $n\lambda=2d\sin\theta$, where n is a positive integer, λ is the wavelength of the incident wave, d is the interplanar distance, and θ is the scattering angle. The interplanar distance (d) and scattering angle (θ) are inversely proportional (a longer interplanar distance produces a smaller scattering angle). It means that the remaining degree of solid solution F490AA and F510AA might be larger than RS490AA and RS510AA. Therefore, the amounts of precipitation for RS490AA and RS510AA are greater than those for F490AA and F510AA, resulting in higher tensile strength and lower tensile ductility. (4) The effect of grain size: after T6 heat treatment, the average grain sizes of as-received tubes (F490AA and F501AA) were larger than those of as-swaged tubes (R490AA and R510AA). When the average grain size is smaller, the density of grain boundaries is higher.

Precipitating phases more easily nucleate on grain boundaries due to inhomogeneous nucleation (low free energy). Grain boundaries can restrict dislocation slipping as deformation. Therefore, a high density of dislocations enhances tensile strength. Furthermore, grain boundaries are diffusive routes for eutectic phases solutionizing into the matrix. This may explain why the eutectic phase fractions of as-swaged 2024 tubes are lower than those of as-received 2024 tubes before and after T6 heat treatment, as shown in Figs. 8 and 9. A higher degree of solid solution leads to stronger precipitation hardening.

Table 3 Residual stress of alloys

Material code	Residual stress (MPa)
F	-20.8
RS	35.2
F510AA	-4.0
RS510AA	16.2

+ : tensile stress; - : compressive strss

Figure 17 shows the tensile fracture characteristics of six specimens. For RS, the fracture surface is flatter than that for other specimens. Some cleavages, a tensile brittle fracture characteristic, appear on the fracture surface. Even though there are some dimple-like structures on the surface, they are very shallow. The features of a fracture surface result from brittle fracture. A lot of dimples appear in the F, F490AA, F510AA, RS490AA, and RS510AA specimens. Micro-void coalescence and ductile fracture caused these dimple fractures. Large dimples initiate at eutectic particles and small dimples initiate at precipitating phases. The particles in the large dimples are Al_2CuMg and $Al_7Cu_2Fe(Mn)$, as determined using EDS of SEM. Dimple fracture is a ductile fracture characteristic. It shows that these fives specimens experienced ductile fracture even though the elongation of RS490AA and RS510AA is slightly lower than that of the others. In general, brittle fracture should be avoided because it leads to low fracture toughness. Suitable heat treatment can make as-swaged tubes have high mechanical strength (especially YS) and sufficient toughness.

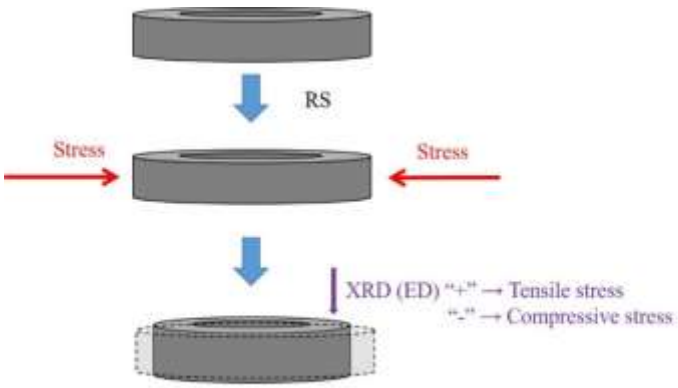

(a)

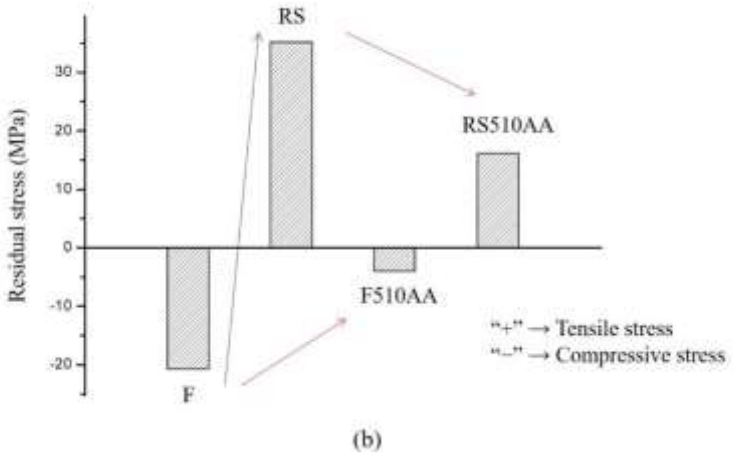

Fig. 15 (a) Illustration of residual tensile stress and compressive stress and (b) residual stress.

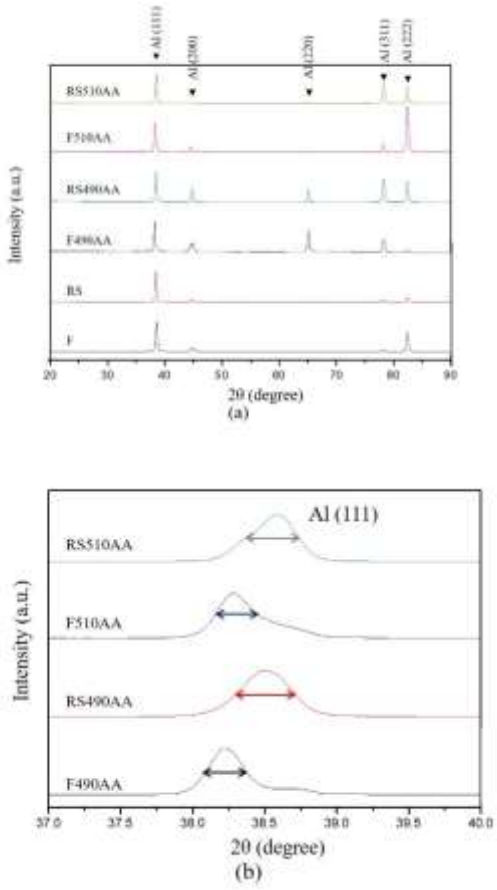

Fig. 16 XRD patterns of materials: (a) from 20° to 90° and (b) around (111) peak.

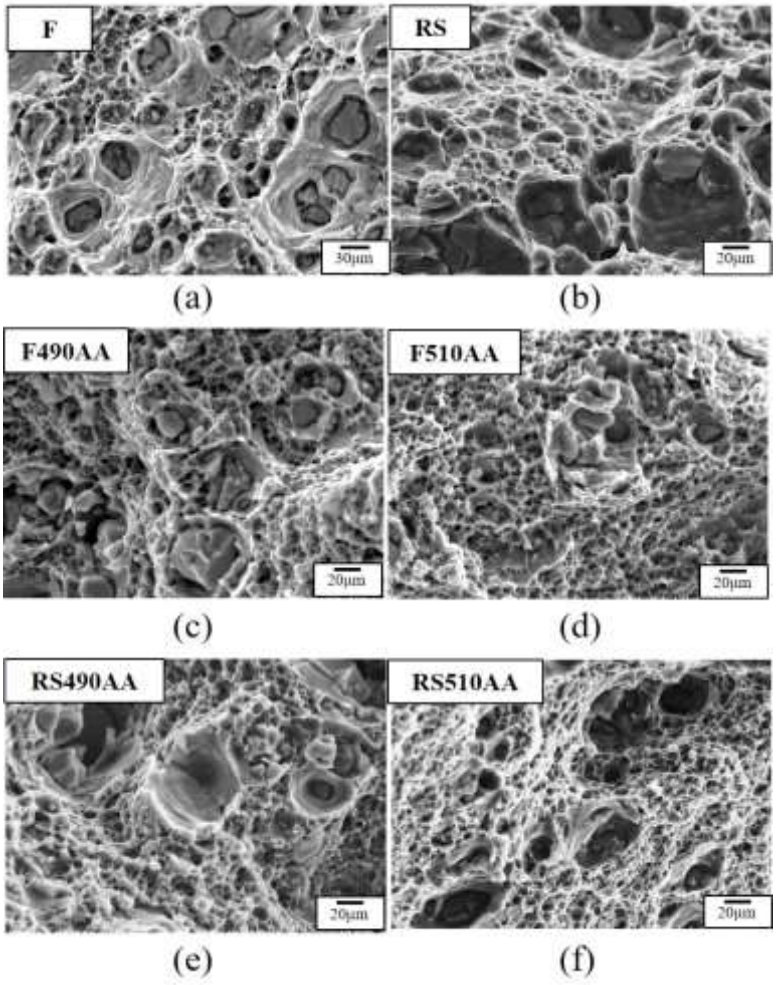

Fig. 17 SEM images of tensile fracture surface of (a) F, (b) RS, (c) F490AA, (d) F4510AA, (e) RS490AA, and (f) RS510AA

Conclusion

The following conclusions are drawn based on the obtained results.

1. The optimal T6 heat treatment conditions for as-received 2024 tubes (F) and as-swaged 2024 tubes (RS) are the same: solid solution at 510 °C and 490 °C for 2 hours each, followed by quenching in water and artificial aging at 210 °C for 3 hours.
2. The rotary swaging process uniformly refines the grain size via dynamic recrystallization and decreases the fraction of eutectic phases. These effects are maintained after T6 heat treatment. The degree of anisotropic microstructural characteristic of initial as-received tubes decreases, but it still exists in as-swaged tubes.
3. The kinds of eutectic phase in the six specimens were identical. The four eutectic phases are Al_2CuMg (S phase), Al_7Cu_2Fe(Mn) (N phase), Mg_2Si (β phase), and Si particles. Both rotary swaging process and T6 heat treatment decrease their fraction.
4. The micro-hardness distribution in as-swaged tubes is not uniform, but T6 heat treatment makes it uniform. After T6 heat treatment, tensile strength increases and tensile elongation decreases. Higher solid solution temperature leads to higher tensile strength. The as-swaged tubes had higher tensile strength than that of as-received tubes. The tensile strength of RS510AA was the highest despite the existence of some partial melting voids.
5. The rotary swaging process enhances tensile strength. The YS of as-swaged tubes greatly improved after T6 heat treatment. This indicates that T6-heat-treated as-swaged 2024 tubes have potential for some structural

components in industrial applications. Even though rotary swaging reduced the ductility of 2024 tubes after T6 heat treatment compared to that of as-received 2024 tubes, the tensile toughness is still sufficiently high for some applications.

6. For the rotary swaging process, the following factors improved mechanical strength before and after T6 heat treatment: (1) remaining residual stress, (2) internal defects, (3) higher amounts of precipitating phases, and (4) finer grain size. This research shows that in addition to reducing size, rotary swaging process is an affective process for improving mechanical strength, especially YS

References

[1] M. A. Abdulstaar, E. A. El-Danaf, N. S. Waluyo, L. Wagner, Severe plastic deformation of commercial purity aluminum by rotary swaging: Microstructure evolution and mechanical properties. Materials Science and Engineering, 2013. 565: pp. 351-358.
[2] E. Rauschnabel, V. Schmidt, Modern applications of radial forging and swaging in the automotive industry. Materials Processing Tenchnology, 1992: pp. 371-383.
[3] D. Rippel, E. Moumi, M. Lütjen, B. Scholz-Reiter, and B. Kuhfuß2, Application of Stochastic Regression for the Configuration of Microrotary Swaging Processes. Mathematical Problems in Engineering, 2014: pp. 1-12.
[4] S. J. Lima, H. J. Choia, C. H. Leeb, Forming characteristics of tubular product through the rotary swaging process. Journal of Materials Processing Technology, 2009: pp. 283-288.
[5] M. A. Abdulstaar, E. A. El-Danaf, N. S. Waluyo, L. Wagner, Severe plastic deformation of commercial purity aluminum by ratary swaging: microstructure evolution an mechanical properties. Materials Science and Engeering: A, 2013, 565, pp.351-358.
[6] W. M. Gan, Y. D. Huang, R. Wang, Z. Y. Zhong, N. Hort, K.U. Kainer, N. Schell, H. G. Brokmeier, A. Schreyer, Bulk and local textures of pure magnesium processed by rotary swaging. Journal of Magnesium and Alloys, 2013: pp. 341-345.
[7] M. Abdulstaar, M. Mhaede, M. Wollmann, L. Wagner, Investigating the effects of bulk and surface severe plastic deformation on the fatigue, corrosion behaviour and corrosion fatigue of AA5083. Surface and Coatings Technology, 2014: pp. 244-251.
[8] J.E. Hatch, "Aluminum: properties and physical metallurgy", American Society for Metals, 1984: pp. 397-400.
[9] R. A. Jeniski Jr., “Effects of Cr addition on the microstructure and mechanical behavior of 6061-T6 continuously cast and rolled redraw rod”, Materials Science and Engineering A, 237, pp.52-64, 1997.
[10] S. R. Claves, D. L. Elias, and W. Z. Misiolek, :Analysis of the intermetallic phase transformation occurring during homogenization of 6xxx aluminum alloys”, Materials Science Forum., 396, pp.667-674, 2002.
[11] N. D. Alexopoulos, Z. Velonaki, C. I. Stergious, S. K. Kourjoulis, Effect of aging on precipitation kinetics, tensile and work hardening behavior of Al-Cu-Mg (2024) alloy, Materials Science and Engineering: A, 2017, 700, pp.457-467.
[12] J. Koziel, L. Błaż, G. Włoch, J. Sobota, P. Lobry, Precipitation Processes during Non-Isothermal Ageing of Fine-Grained 2024 Alloy. Archives of Metallurgy and Materials, 2016: pp. 169-176
[13] K. P. Young, C. P. Kyonka, and J. A. Courtois, United States Patent 4415374, Nov.15, 1983.
[14] M. Abdulstaar, M. Mhaede, M. Wollmann, L. Wagner, Investigating the effects of bulk and surface severe plastic deformation on the fatigue, corrosion behaviour and corrosion fatigue of AA5083. Surface and Coatings Technology, 2014: pp. 244-251.
[15] N. Durlu, N. K. Çalişkan, and Ş. Bor, Effect of swaging on microstructure and tensile properties of W–Ni–Fe alloys. International Journal of Refractory Metals and Hard Materials, 2014: pp. 126-131.
[16] M. H. Goodarzy, H. Arabi, M. A. Boutorabi, S. H. Seyedein, S. H. Hasani Najafabadi, The effects of room temperature ECAP and subsequent aging on mechanical properties of 2024 Al alloy. Journal of Alloys and Compounds, 2014: pp. 753-759.
[17] M. Mirzaei, M. R. Roshann, S. A. Jenabali Jahromi, Microstructure and mechanical properties relation in cold rolled Al 2024 alloy determined by X-ray line profile analysis. Materials Science and Engineering: A, 2015: pp. 44-49.

.